

IMPROVING SEISMOGRAMS' RESOLUTION BY USING A PHASE-SHRINKAGE FILTERING METHOD

Milton J. Porsani ^{1,2*}

¹Universidade Federal da Bahia - UFBA, Institute of Geosciences, Salvador, BA, Brazil

²National Institute of Science and Technology of Petroleum Geophysics (INCT-GP/CNPq)

*Corresponding author e-mail: porsani@ufba.br

ABSTRACT. The improvement in the temporal resolution of seismograms is usually achieved by compressing, or deconvolving, the seismic pulse. In this paper, I present a new method of filtering time series that shrinks the positive or negative polarity band of a signal while expands its opposite polarity. The filtering method uses the complex seismic trace to compute the instantaneous phase, which is shrunk around the positions of the local maximum (or minimum) values corresponding to the reflections of the original signal. It calculates the real and imaginary components afterward, thus representing the filtered signal. The method is applied trace-by-trace and promotes a significant improvement in the temporal resolution of the seismograms, revealing in greater detail the reflections and structures of the subsurface. Numerical examples with 2D stacked seismic lines (from the Pelotas Basin, and from the mouth of the Amazon river), and 3D, from the F3Demo of the OpendTect repository, illustrate the performance of the new method proposed here. The average amplitude spectra of the filtered data reveal the presence of the high and low frequency contents in the filtered results.

Keywords: wavelet deconvolution, seismic processing, filtering, complex trace, instantaneous phase

INTRODUCTION

Among geophysical methods, the seismic reflection one is the most used in the exploration of hydrocarbons. It allows, like no other, obtaining an image of the subsurface that clearly reflects the geology of the sedimentary basins. Improving the quality of seismic images and increasing the ability to identify and discriminate the seismic reflectors is one of the biggest challenges of the seismic reflection method. Aiming to improve the resolution, quality and fidelity of seismic imaging, new methods of processing and filtering seismic data are being continuously developed.

In seismic oil exploration, particularly in the study of reservoirs, deconvolution is an important step of seismic processing, applied to improve temporal resolution of traces, allowing better top and bottom identification of thinner layers and thus better definition of subsurface geology. When used for this purpose, it is called wavelet or spiking deconvolution (Treitel and Robinson, 1966; Robinson, 1967; Berkhout, 1977; Wiggins, 1978; Robinson and Treitel, 1980; Ulrych and Walker, 1982; Robinson and Osman, 1996). Wavelet deconvolution aims to compress the wavelet shape in order to recover the reflectivity function or impulse response of the medium. In the last seven

decades, several papers on deconvolution and wavelet estimation have been published in Geophysics literature. Most often the authors focus on and try to solve problems related to the wavelet phase character (Clarke, 1968; Eisner and Hampson, 1990; Ulrych and Treitel, 1991; Lazear, 1993; Leinbach, 1995; Ursin et al., 1996; Porsani and Ursin, 1998, 2000; Ursin and Porsani, 2000; Sacchi and Ulrych, 2000; Misra and Sacchi, 2007; Lü and Wang, 2007; van der Baan, 2008; Misra and Chopra, 2010; Ledesma and Porsani, 2013)

The Wiener spiking deconvolution filter has been developed and applied for seismic data processing (Robinson, 1957; Robinson and Treitel, 1980; Leinbach, 1995; Yilmaz, 2001), with the assumptions that the reflectivity series have the statistical properties of random white noise and the wavelet is minimum-phase. The ability of this filter to compress the seismic wavelet in time, despite these questionable assumptions, is responsible for the popularity of the Wiener spiking deconvolution technique in the petroleum industry. It is well known that minimum-phase seismic deconvolution performs poorly when the seismic pulse is mixed phase (Robinson, 1967; Robinson and Treitel, 1980; Leinbach, 1995; Lang, 1998; Yilmaz, 2001)

Several alternative approaches have been proposed to bypass the minimum-phase restriction of the conventional Wiener spiking filter. Ziolkowski and Slob (1991) discuss the use of polynomial factorization to perform deconvolution. They conclude that it is impossible to identify and extract the true source signature from measured seismic data without using assumptions about the statistical properties of the impulse response of the earth. Ulrych et al. (1995) presented two different methods for statistical wavelet estimation. The first, based on cepstral stacking and homomorphic decomposition, does not demand any assumption concerning the statistical properties of the reflectivity. The second method uses a global optimization scheme with the constraint that the reflectivity is a non-Gaussian, stationary, and statistically independent random process. Porsani and Ursin (1998, 2000) presented a mixed-phase deconvolution method, by using the solution of Yule-Walker equations to estimate the polynomial roots associated with the minimum-phase wavelet and then obtained mixed-phase filters using all-pass operators. Ledesma and Porsani (2013) uses the roots of these polynomials to obtain an optimum inverse filter via genetic algorithm. Misra and Sacchi (2007) and Misra and Chopra (2010) deconvolve the data with a standard spiking deconvolution filter. From the filtered, whitened data, they estimate an all-pass phase filter, which is then applied to the whitened data.

In this paper I present a new approach to increase the temporal and spatial resolution of the seismic data, which is based on the shrinkage of the instantaneous phase of the complex seismograms (Taner et al., 1979).

THE PHASE-SHRINKAGE FILTERING METHOD

Let $D(t)$ represent the complex seismic trace (Taner et al., 1979),

$$D(t) = d(t) + i\mathcal{H}\{d(t)\}, \quad (1)$$

where, $d(t)$ is the real seismic trace and $\mathcal{H}\{\cdot\}$ denotes the Hilbert transform,

$$\mathcal{H}\{d(t)\} = \tilde{d}(t) = \frac{1}{\pi} \int_{-\infty}^{\infty} \frac{d(\tau)}{t - \tau} d\tau. \quad (2)$$

The real and imaginary parts of equation 1 are equal to,

$$d(t) = A(t) \cos \theta(t), \quad (3)$$

$$\tilde{d}(t) = A(t) \sin \theta(t) \quad (4)$$

where $A(t)$ represent a time-dependent amplitude, “instantaneous amplitude”, and $\theta(t)$ is the time-dependent phase, “instantaneous phase”, (Bracewell,

1965),

$$A(t) = \sqrt{d(t)^2 + \tilde{d}(t)^2}, \quad (5)$$

$$\theta(t) = \arctan \left[\frac{\tilde{d}(t)}{d(t)} \right]. \quad (6)$$

The instantaneous phase is responsible for the shape of the signal and, by shrinking the phase, it is possible to squeeze in time the shape of the reflection. The idea is to shrink the phase around the local maximum, or local minimum, values of the signal, such that the wavelets corresponding to the reflections could occur in a short time interval. That may be done by using the following equation, adapted from the very fast simulated annealing method (Sen and Stoffa, 1995),

$$\theta^\xi(t) = \pi \operatorname{sgn}[\theta(\xi, t)] T \left[\left(1 + \frac{1}{T} \right)^{\frac{|\theta(\xi, t)|}{\pi}} - 1 \right]. \quad (7)$$

Here the parameter T , ($T < 1$), controls the degree of the phase-shrinkage. The symbol ξ , assumes values equal to $\{+1, -1\}$, according to the positive or negative polarity of the original signal, chosen to be shrunk. $\operatorname{sgn}[\cdot]$ is the function that collects the sign of the instantaneous phase of the complex signal. The variable $\theta(\xi, t)$, $[-\pi \leq \theta(\xi, t) \leq \pi]$, is the instantaneous phase which depends on the ξ value,

$$\theta(\xi, t) = \xi \arctan \left[\frac{\xi \tilde{d}(t)}{-\xi d(t)} \right]. \quad (8)$$

The new complex and filtered seismic trace is,

$$D^\xi(t) = d^\xi(t) + i \tilde{d}^\xi(t), \quad (9)$$

where its real and imaginary components are given by,

$$d^\xi(t) = A(t) [-\xi \cos \theta^\xi(t)], \quad (10)$$

$$\tilde{d}^\xi(t) = A(t) \sin \theta^\xi(t). \quad (11)$$

Both the instantaneous amplitudes, $A(t)$, of the filtered, and the original complex seismic traces are the same.

Here are the Fortran steps of the proposed phase-shrinkage filtering method:

```

xi = 1.    ! or -1. to shrinkage of the minima values
T = 0.01
pi = acos(-1.)
W = 1. + 1./T
call cmplx_trace(ns,d,cx)      ! Complex trace, cx
Amp = abs(cx)                  !Eq.(5)
pha = xi*atan2(xi*aimag(cx),-xi*real(cx)) !Eq.(8)

do i=1,ns ! loop over the time samples
  signal=sign(1.,pha(i))
  pha_mod(i)=pi*signal*T*(W**abs(pha(i)/pi)-1.) !Eq.(7)
  filt_c(i)=Amp(i)*(-xi*cos(pha_mod(i))) !Eq.(10)
  filt_s(i)=Amp(i)*sin(pha_mod(i)) !Eq.(11)
enddo

```

Figure 1 illustrates the effect of the magnitude of the T parameter in the phase-shrinkage method, by using a complex cosenosoid function. The real and imaginary parts of the complex signal are shown in (a) and (b), respectively. The phase computed using equation 8, for $\xi = +1$, is shown in (c). The phase-shrinkage for $T = \{10^{-9}, 10^{-6}, 10^{-2}, 10^{-1}, 1\}$ is shown from (d) to (h). The shrinkage may be observed more effectively for smaller values of T.

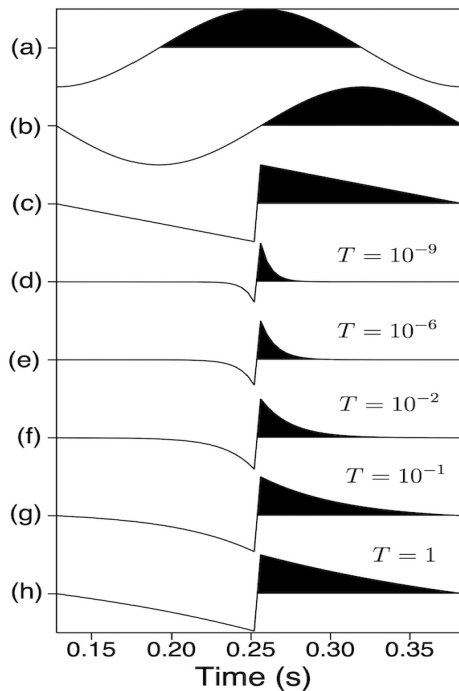


Figure 1: The phase shrinkage for different values of the T parameter. The real and imaginary parts of a cosenosoid complex signal are shown in (a) and (b), respectively. The phase computed using equation 8, for $\xi = +1$, is shown in (c). The effect in the phase shrinkage for different values of the T parameter is shown from (d) to (h).

Figure 2 illustrates the results obtained by using equations 7 to 11, when associated with the phase-shrinkage of the local maxima ($\xi = +1$) of the original signal. The parameter T was set as $T = 0.00001$. A cosenosoid function is represented in (a) and its normalized instantaneous phase, associated to equation 8, in (b). The shrunk phase computed by using equation 7, with normalized values, is shown in (c), and the real and imaginary components of the new complex signal are represented in (d) and (e), respectively. The real component, (d), shows the time-squeezing of the band of positive values of the input signal, at the local maxima, and the expansion of the negative ones, around the local minima. In the imaginary component, (e), only the shrinkage of the positive polarity of the input signal is present. The instantaneous amplitude, equal to the input data and the filtered ones, is shown in (f).

Figure 3 illustrates the results obtained by using

equations 7 to 11, associated with the phase-shrinkage of the local minima ($\xi = -1$) of the original signal. The normalized instantaneous phase, associated with equation 8, is shown in (b). The shrunk phase computed by using equation 7, with normalized values, is shown in (c). The real component of the new complex signal is represented in (d), where the negative polarity of the input signal was shrunk while the positive one was expanded. The imaginary component, (e), shows the contraction of the negative portion of the signal, corresponding to the local minima of the input signal.

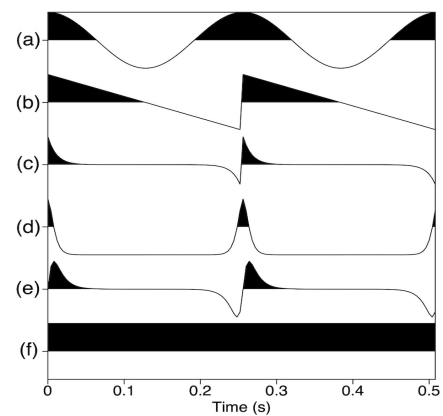


Figure 2: Shrinkage of the positive polarity of the signal. A cosenosoid function is represented in (a). The instantaneous phase computed by using equation 8 is shown in (b). The shrinkage phase is shown in (c), and the real and imaginary components of the new complex signal are represented in (d) and (e), respectively. The instantaneous amplitude is shown in (f).

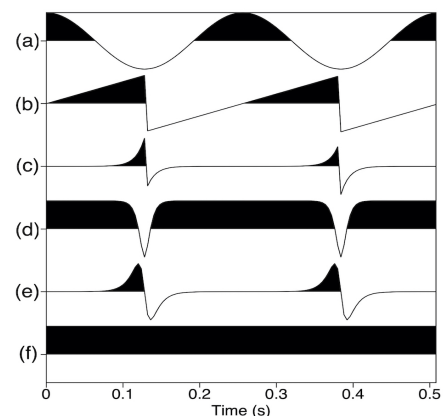


Figure 3: Shrinkage of the negative polarity of the signal. A cosenosoid function is represented in (a) and its instantaneous phase, computed with equation 8, is shown in (b). The shrinkage phase is shown in (c). The real component of the filtered signal is shown in (d). The negative polarity of the input signal was shrunk while the positive one was expanded. The imaginary component, (e), shows the contraction of the negative portions of the signal, corresponding to the local minima of the input signal. The instantaneous amplitude is shown in (f).

Figures 4 and 5 show the shrinkage of the positive polarity ($\xi = +1$) of a real seismic trace of post-stacked data, by using different values of T. The real seismic trace and its Hilbert transform are shown in (a) and (b), and the instantaneous amplitude in (i). From (c) to (h) of Figure 4 the real components of the filtered data are shown associated with $T=(10^{-7}, 10^{-5}, 10^{-3}, 10^{-2}, 10^{-1}, 1)$, respectively. The effect of the smaller values of the T parameter on the shrinkage of the band of polarity may be observed, corresponding to the maximum local values of the original seismic trace. Similar results are observed in the imaginary components shown from (c) to (h) of Figure 5.

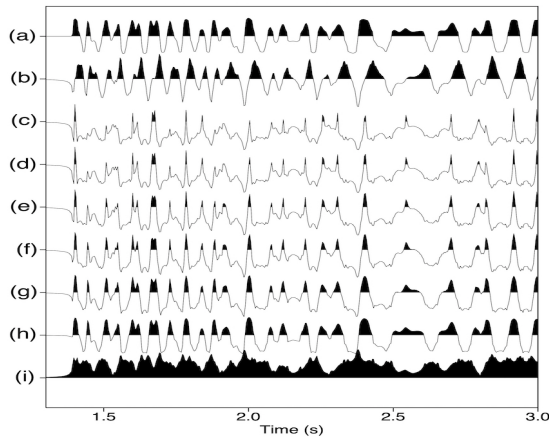


Figure 4: Shrinkage of the positive polarity of a seismic trace, by using different values of the parameter T. A real seismic trace is shown in (a) and its Hilbert transform in (b). The real components of the filtered data are shown from (c) to (h) by using $T=(10^{-7}, 10^{-5}, 10^{-3}, 10^{-2}, 10^{-1}, 1)$, respectively. The instantaneous amplitude is shown in (h).

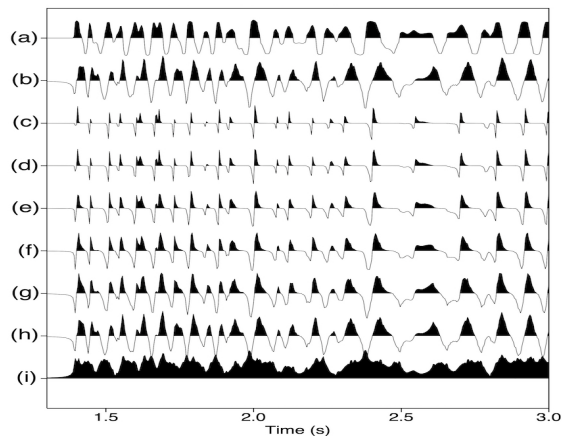


Figure 5: Shrinkage of the positive polarity of a seismic trace, by using different values of the parameter T. A real seismic trace is shown in (a) and its Hilbert transform in (b). The imaginary components of the filtered data are shown from (c) to (h) by using $T=(10^{-7}, 10^{-5}, 10^{-3}, 10^{-2}, 10^{-1}, 1)$, respectively. The instantaneous amplitude is shown in (h).

Figures 6 and 7 show the shrinkage of the negative polarity ($\xi = -1$) of the real seismic trace, by using different values of T. The real seismic trace, its Hilbert transform, and the instantaneous amplitude are shown in (a), (b), and (i). From (c) to (h) of Figure 6 are shown the real components of the filtered data are shown associated with $T=(10^{-7}, 10^{-5}, 10^{-3}, 10^{-2}, 10^{-1}, 1)$, respectively. The effect of the smaller values of the T parameter on the shrinkage of the band of polarity may be observed, corresponding to the minimum local values of the original seismic trace. Similar results are observed in the imaginary components shown from (c) to (k) in Figure 7.

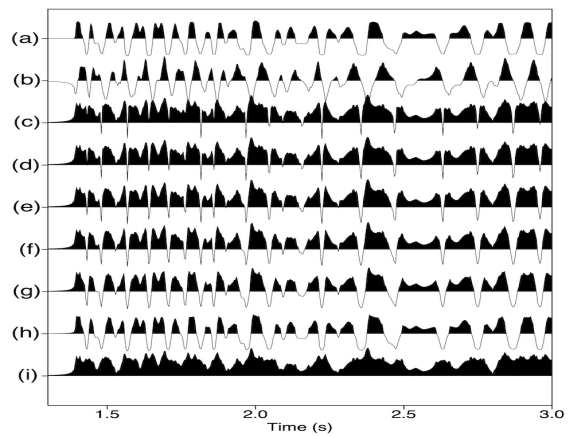


Figure 6: Shrinkage of the negative polarity of a seismic trace, by using different values of the parameter T. A real seismic trace is shown in (a) and its Hilbert transform in (b). The real components of the filtered data are shown from (c) to (h) by using $T=(10^{-7}, 10^{-5}, 10^{-3}, 10^{-2}, 10^{-1}, 1)$, respectively. The instantaneous amplitude is shown in (h).

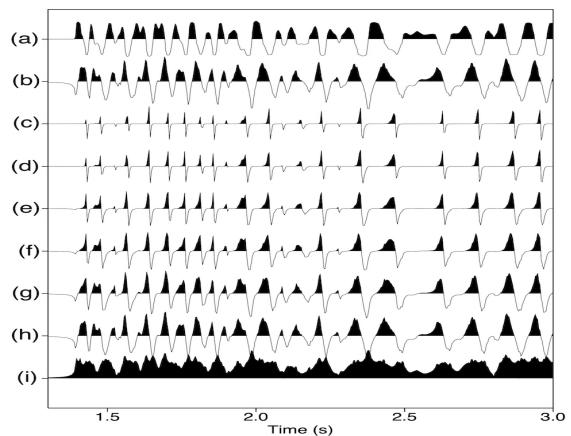


Figure 7: Shrinkage of the negative polarity of a seismic trace, by using different values of the parameter T. A real seismic trace is shown in (a) and its Hilbert transform in (b). The imaginary components of the filtered data are shown from (c) to (h) by using $T=(10^{-7}, 10^{-5}, 10^{-3}, 10^{-2}, 10^{-1}, 1)$, respectively. The instantaneous amplitude is shown in (h).

NUMERICAL EXAMPLES

Numerical examples with stacked seismic - 2D from the mouth of the Amazon river, and from the Pelotas Basin - and, 3D from F3Demo, illustrate the obtained results with the new method. In the following examples I chose to shrink the positive polarity (black color) of the input seismic traces.

Figure 8 shows a post-stacked seismic line of the mouth of the Amazon river. Figure 9 shows the real part of the filtered data. The enhancement of the temporal and spatial resolution is clearly seen in the image. Figure 10 shows the filtered data corresponding to the imaginary part of the complex traces. In this case, as presented in Figures 1e and 2e, the interfaces between layers are clearly displayed. The residue between the original data and the results depicted in Figure 9 is shown in Figure 11. Figure 18 shows the average amplitude spectra of the original and the filtered data shown in Figure 9 (red line), in Figure 10 (black line), and in Figure 11 (green line). The enhancement of the high frequency content is noted in the real component (Filtered c, red line) and in the imaginary ones (Filtered s, black line). The enhancement of the low frequency content associated to the real component is also evident.

Figure 12 shows a post-stacked seismic line of the Pelotas Basin. Figure 13 shows the real part of the filtered data. The enhancement of both the temporal and spatial resolution is clearly seen in the image. The sub-vertical faults and fractures are better displayed. Figure 14 shows the filtered data corresponding to the imaginary part of the complex traces. Only the interfaces between layers are displayed. Figure 19 shows the average amplitude spectra of the original, and the filtered data shown in Figure 13 (red line), and in Figure 14 (black line). The enhancement of the high frequency content is noted in the real component (Filtered c, red line) and in the imaginary ones (Filtered s, black line). The enhancement of the low frequency content associated to the real component is also evident.

Marine seismic data for the F3 block, North Sea, from the OpendTect repository, is shown in Figure 15 which shows 3D seismic data of the F3Demo. Figures 16 and 17 show the filtered data, and correspond to the real and imaginary components, respectively, of the phase-shrinkage filtering method. The enhancement of the temporal and spatial resolution is clearly shown in the faces of the volume. Figure 20 shows the average amplitude spectra of the original and the filtered data shown in Figure 16 (red line) and in Figure 17 (black line). The enhancement of the high frequency content is evident in the real component (Filtered c, red line) and in the imaginary ones (Filtered s, black line). The enhancement of the low frequency content associated to the real component is also evident.

CONCLUSION

I present a new filtering method, which is quite effective in enhancing the temporal and spatial resolution in seismic images. It is based on a single equation only that is used for changing the instantaneous phase of the complex seismic trace, thus preserving its instantaneous amplitude. The method works trace-by-trace, and its implementation and use are relatively simple and computationally efficient. Its efficacy was demonstrated by filtering 2D and 3D post-stacked seismic data, and the numerical results show significant improvement in the temporal and spatial resolution of seismic events in seismic images. The average amplitude spectra associated with the three examples show the capability of the proposed phase-shrinkage filtering method to recover lower and higher frequency contents corresponding to the reflected events in the seismic data.

DATA AVAILABILITY

I analyzed post-stacked data obtained from the BDEP/ANP repository (Technical Data for Exploration and Production Data Bank / Brazilian National Agency of Petroleum, Natural Gas and Biofuels). Also, I used the marine seismic data for the F3 block, North Sea, from the OpendTect repository, at <https://terranubis.com/datainfo/F3-Demo-2020>.

ACKNOWLEDGMENTS

The author would like to thank INCT-GP/CNPq/MCTI, National Institute of Science and Technology of Petroleum Geophysics (INCT-GP/CNPq/MCTI), CAPES (Coordination for the Improvement of Higher Education Personnel), ANP (Brazilian National Agency of Petroleum, Natural Gas and Biofuels), FINEP (Funding Agency for Studies and Projects), and FAPESB (Bahia State Research Support Foundation) for financial support.

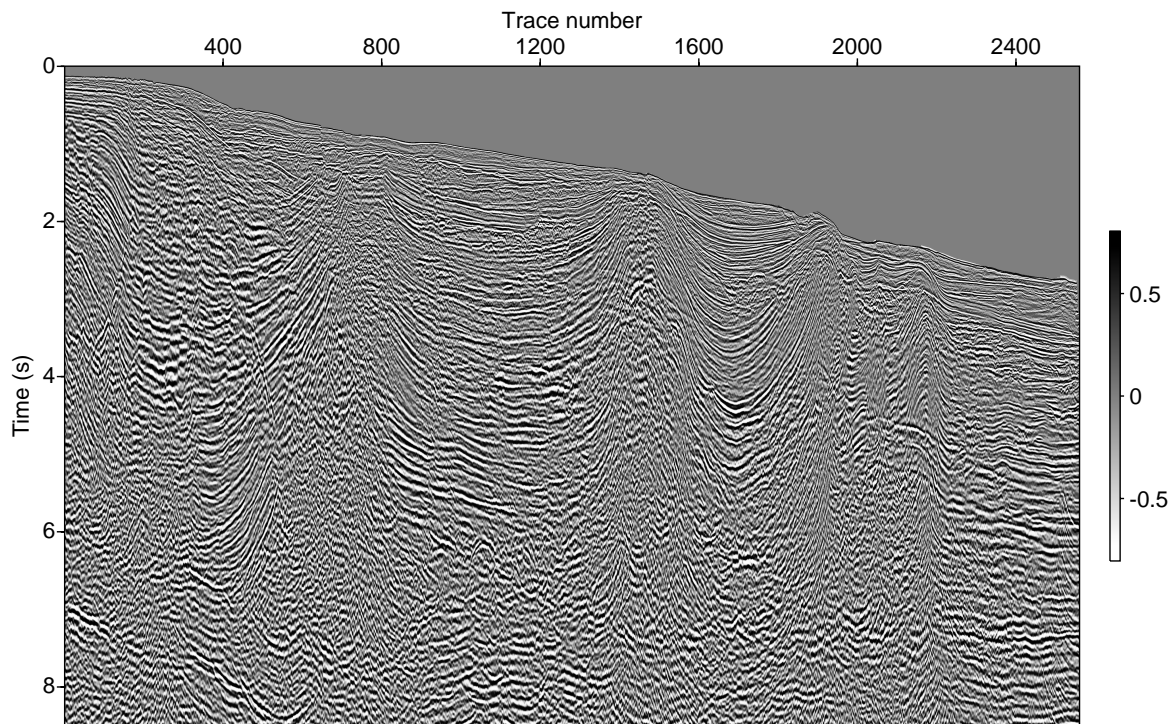


Figure 8: A post-stacked seismic line of the mouth of the Amazon river.

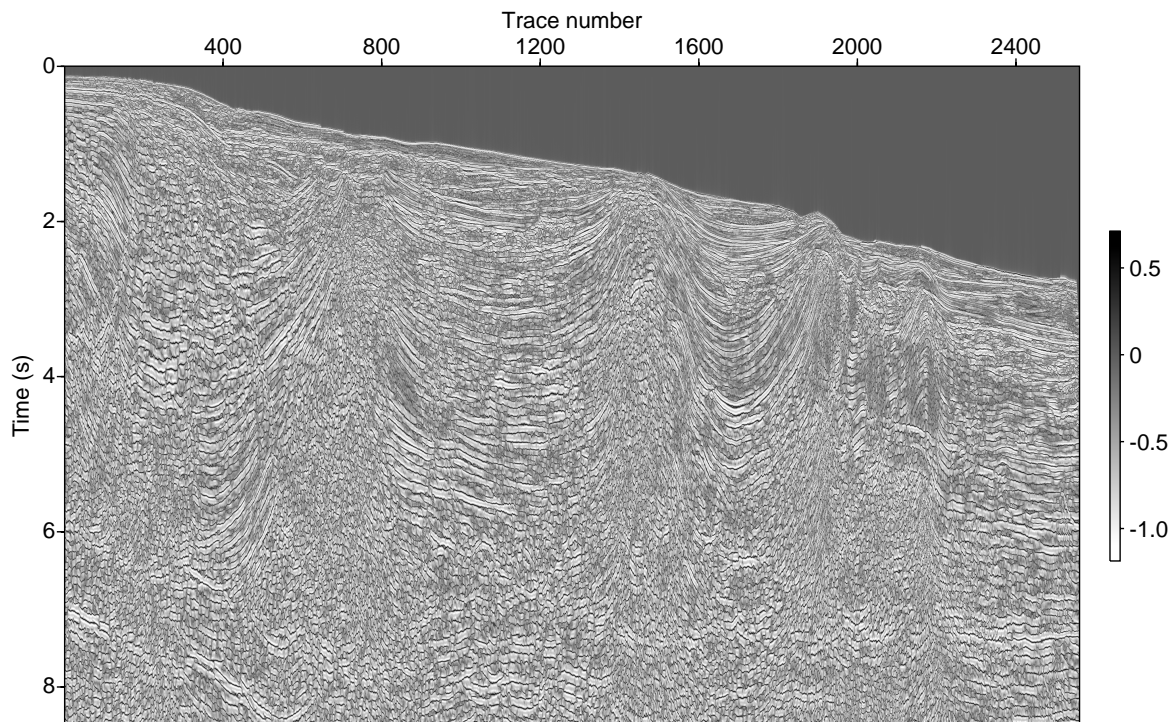


Figure 9: The filtered data corresponding to the real part of the complex seismic traces. The enhancement of the temporal and spatial resolution is clearly seen in the image.

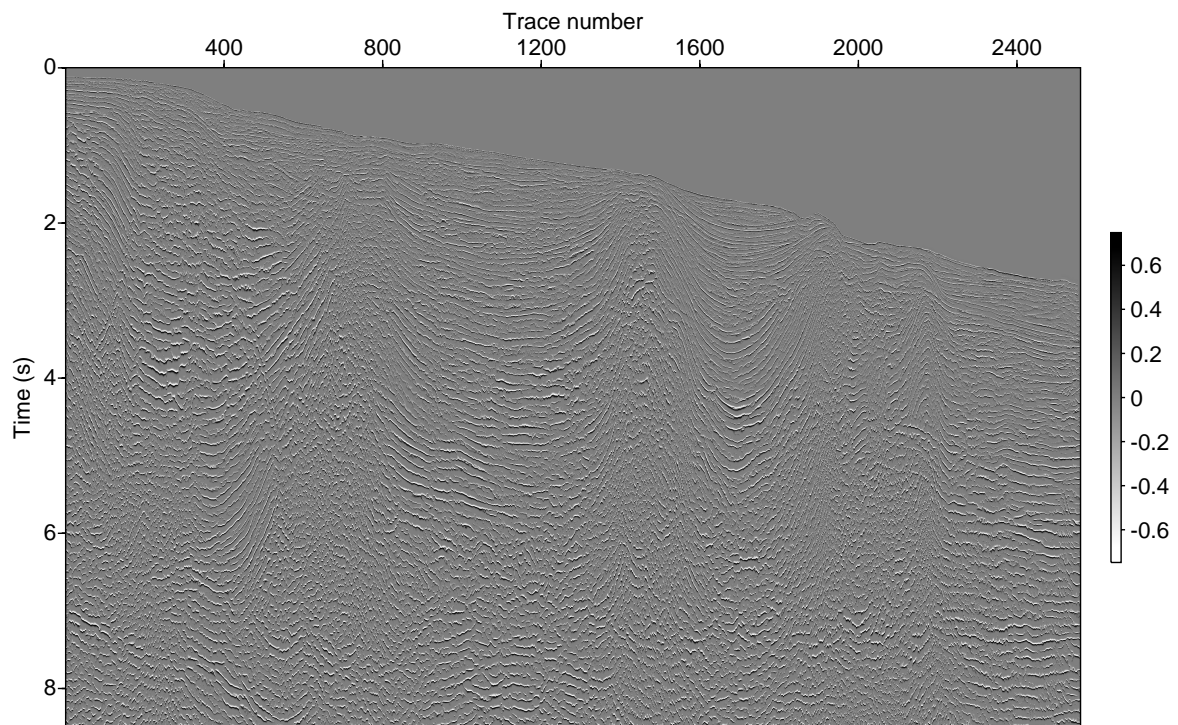


Figure 10: The filtered data corresponding to the imaginary part of the complex seismic traces. The interfaces between layers are clearly enhanced.

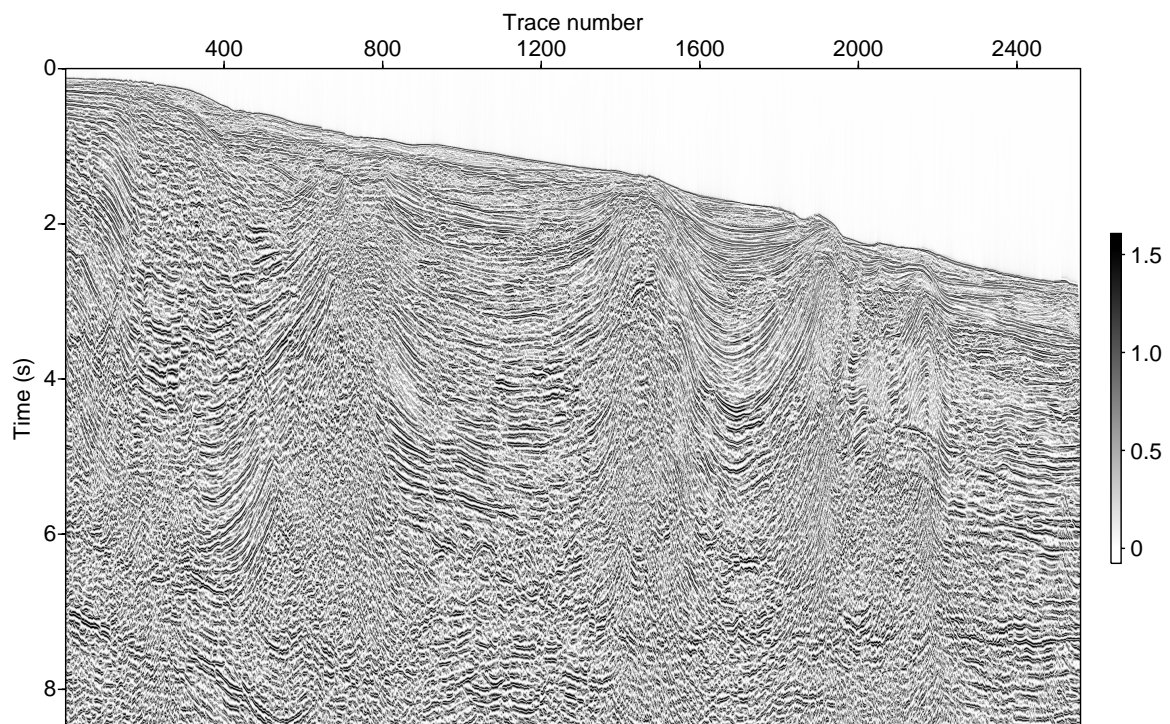


Figure 11: The residue between the original data, (Fig. 8), and the filtered results depicted in Figure 9.

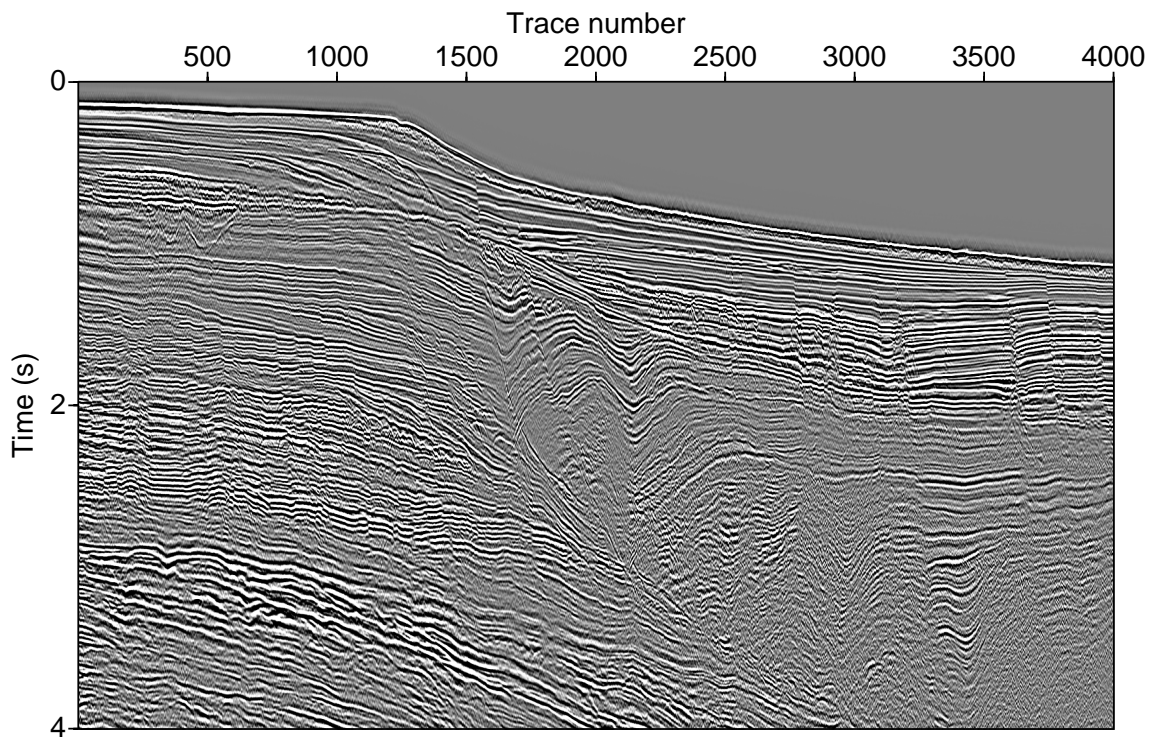


Figure 12: A post-stacked seismic line of the Pelotas Basin.

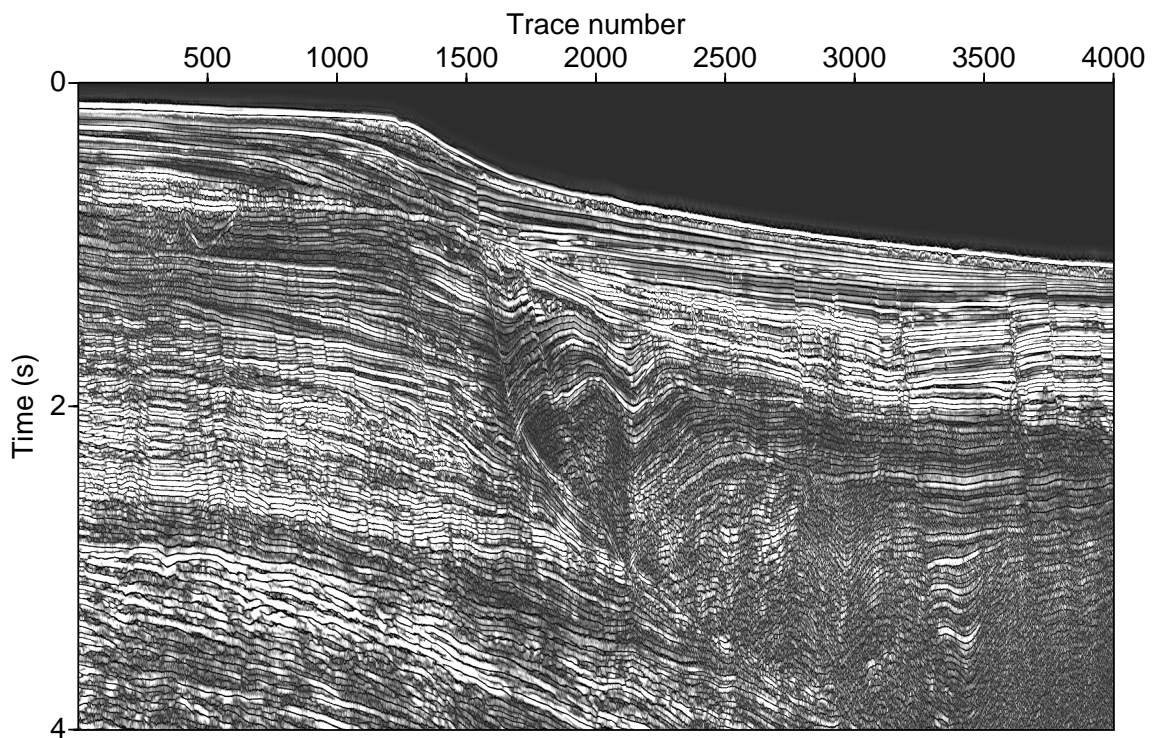


Figure 13: The real part of the filtered data. The enhancement of both the temporal and spatial resolution is clearly seen in the image. The sub-vertical faults and fractures are better displayed.

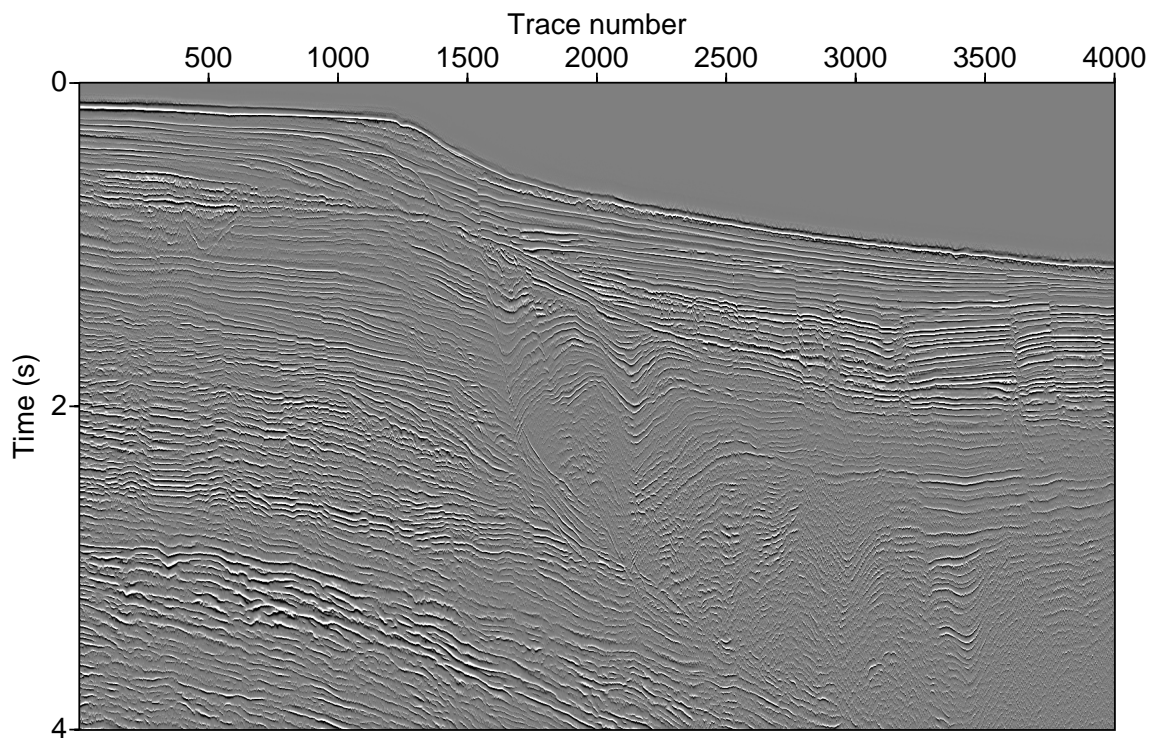


Figure 14: The filtered data corresponding to the imaginary part of the complex traces. The interfaces associated to the layers are enhanced.

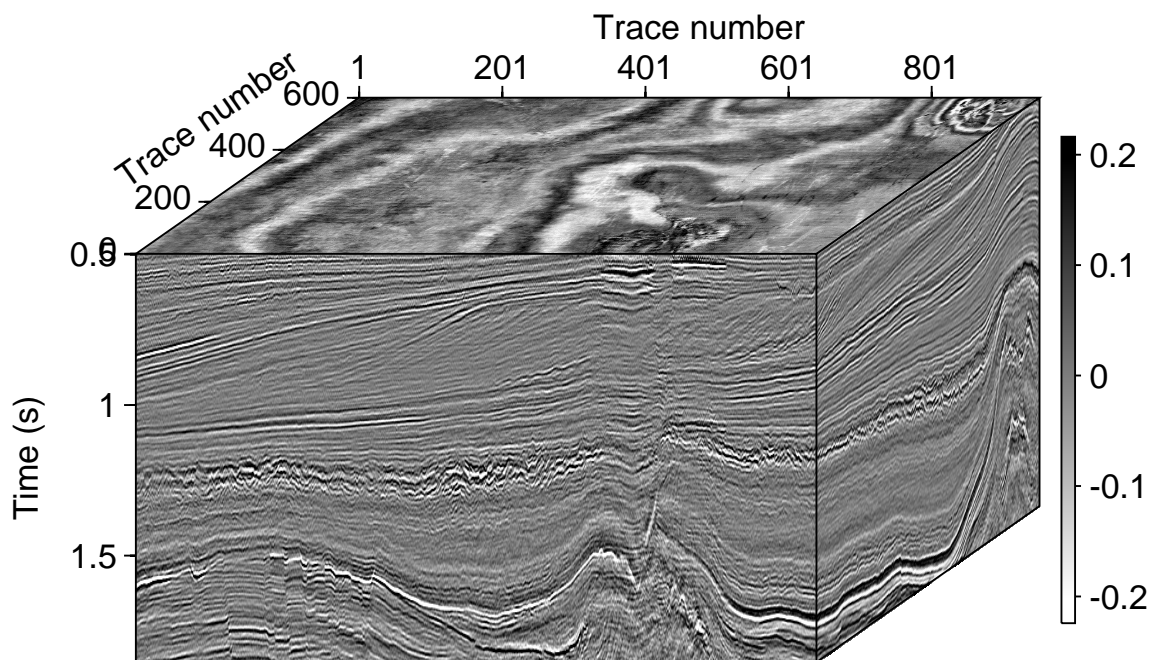


Figure 15: A 3D seismic data of the F3Demo.

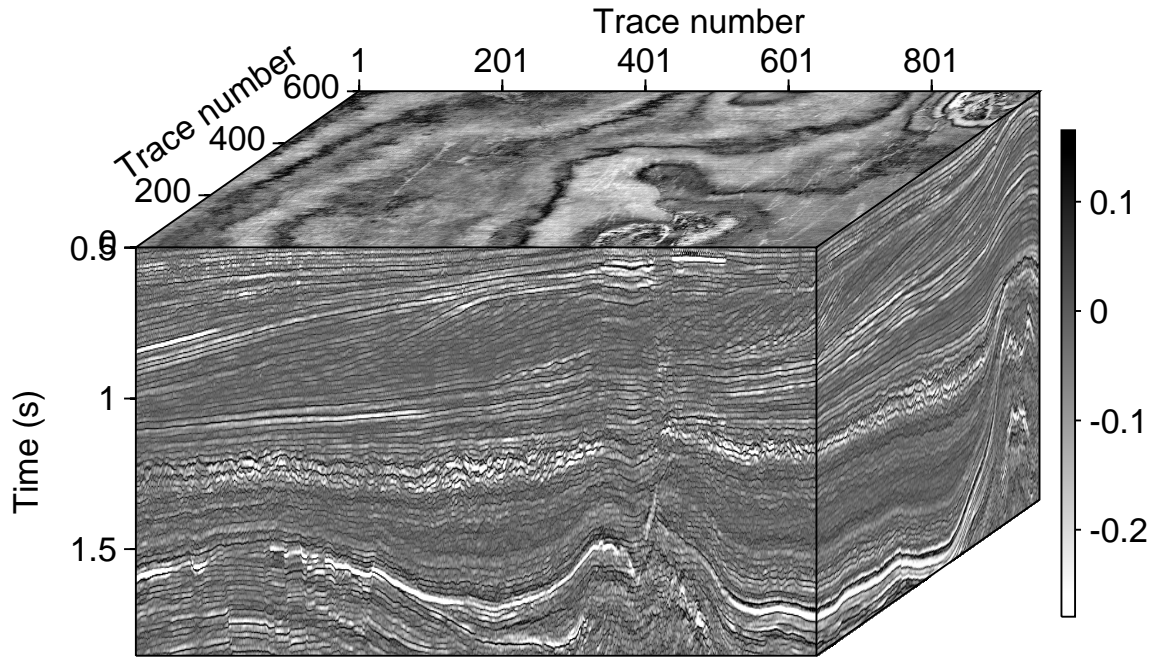


Figure 16: The filtered data correspond to the real component of the phase-shrinkage filtering method. The enhancement of the temporal and spatial resolution is clearly shown in the faces of the volume.

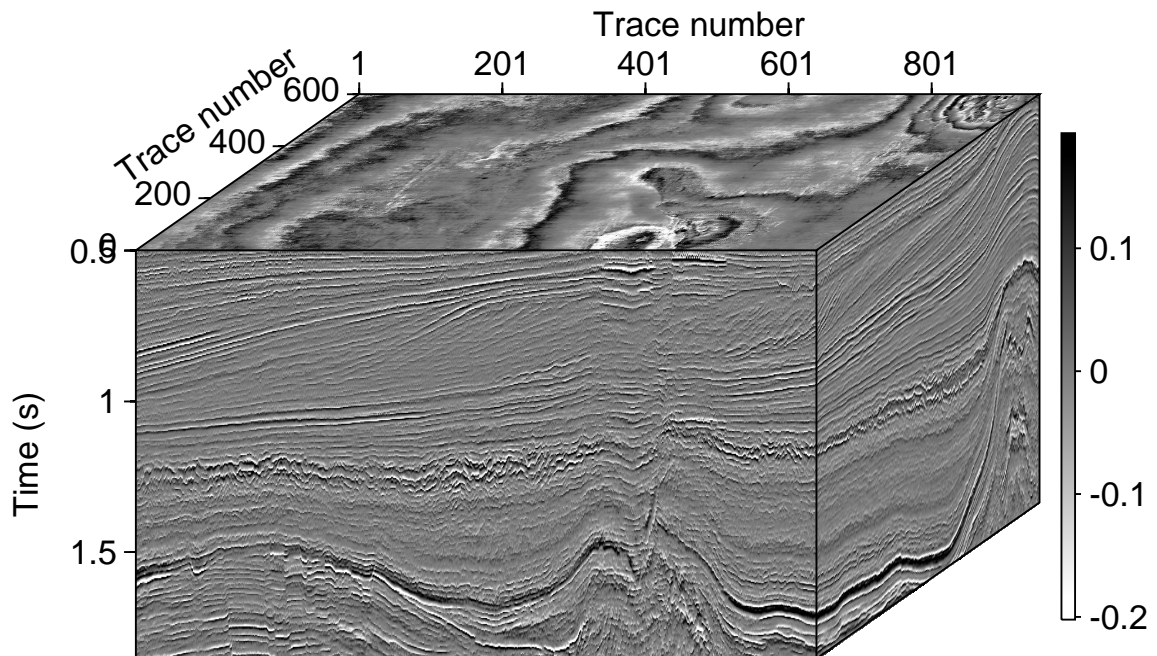


Figure 17: The filtered data correspond to the imaginary component of the phase-shrinkage filtering method. The enhancement of the temporal and spatial resolution is clearly shown in the faces of the volume.

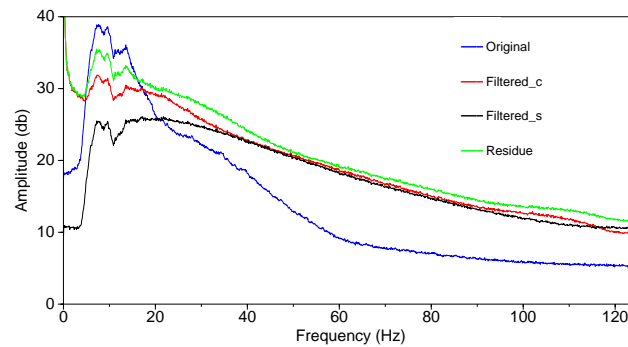


Figure 18: The average amplitude spectra of the original and the filtered data shown in Figure 9 (red line), in Figure 10 (black line), and in Figure 11 (green line). The enhancement of the high frequency content is noted in the real component (Filtered c, red line) and in the imaginary ones (Filtered s, black line). The enhancement of low frequency content associated to the real component is also evident.

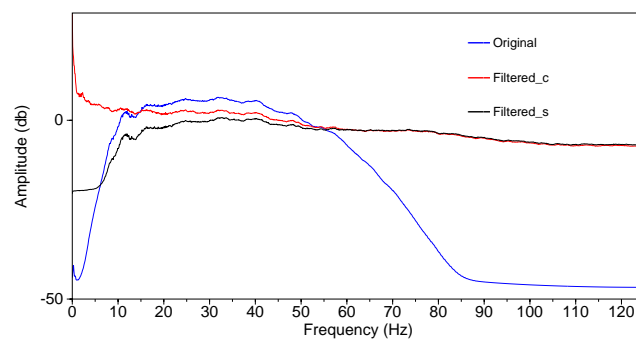


Figure 19: The average amplitude spectra of the original, and the filtered data shown in Figure 13 (red line), and in Figure 14 (black line). The enhancement of the high frequency content is noted in the real component (Filtered c, red line) and in the imaginary ones (Filtered s, black line). The enhancement of the low frequency content associated to the real component is also evident.

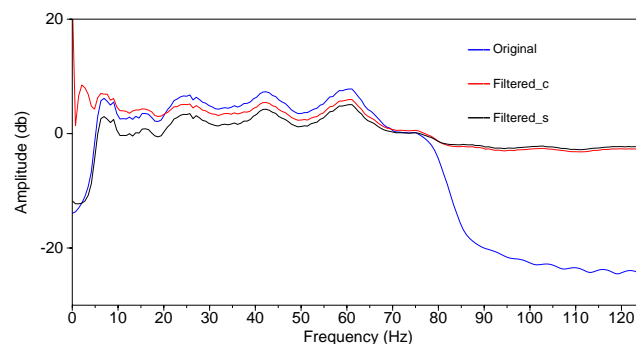


Figure 20: The average amplitude spectra of the original and the filtered data shown in Figure 16 (red line) and in Figure 17 (black line). The enhancement of the high frequency content is evident in the real component (Filtered c, red line) and in the imaginary ones (Filtered s, black line). The enhancement of the low frequency content associated to the real component is also evident.

REFERENCES

- Berkhout, A. J., 1977, Least-squares inverse filtering and wavelet deconvolution: *Geophysics*, **42**, 1369–1383, doi: [10.1190/1.1440798](https://doi.org/10.1190/1.1440798).
- Bracewell, R. N., 1965, *The Fourier Transform and Its Applications*: McGraw-Hill.
- Clarke, G. K. C., 1968, Time-varying deconvolution filters: *Geophysics*, **33**, 936–944, doi: [10.1190/1.1439987](https://doi.org/10.1190/1.1439987).
- Eisner, E., and G. Hampson, 1990, Decomposition into minimum and maximum phase components: *Geophysics*, **55**, 897–901, doi: [10.1190/1.1442904](https://doi.org/10.1190/1.1442904).
- Lang, M., 1998, Allpass filter design and applications: *IEEE Transactions on Signal Processing*, **46**, 2505–2514, doi: [10.1109/78.709538](https://doi.org/10.1109/78.709538).
- Lazear, G. D., 1993, Mixed-phase wavelet estimation using fourth-order cumulants: *Geophysics*, **58**, 1042–1051, doi: [10.1190/1.1443480](https://doi.org/10.1190/1.1443480).
- Ledesma, D. C., and M. J. Porsani, 2013, DECONVOLUTION OF SEISMIC DATA USING PHASE CHANGE OPERATORS: *Brazilian Journal of Geophysics*, **31**, 59–73, doi: [10.22564/rbgf.v31i1.246](https://doi.org/10.22564/rbgf.v31i1.246).
- Leinbach, J., 1995, Wiener spiking deconvolution and minimum-phase wavelets: A tutorial: *The Leading Edge*, **14**, 189–192, doi: [10.1190/1.1437110](https://doi.org/10.1190/1.1437110).
- Lü, X., and Y. Wang, 2007, Mixed-phase wavelet estimation by iterative linear inversion of high-order statistics: *Journal of Geophysics and Engineering*, **4**, 184–193, doi: [10.1088/1742-2132/4/2/007](https://doi.org/10.1088/1742-2132/4/2/007).
- Misra, S., and S. Chopra, 2010, Phase stability via nonlinear optimization: A case study: *The Leading Edge*, **29**, 1338–1343, doi: [10.1190/1.3517304](https://doi.org/10.1190/1.3517304).
- Misra, S., and M. D. Sacchi, 2007, Non-minimum phase wavelet estimation by non-linear optimization of all-pass operators: *Geophysical Prospecting*, **55**, 223–234, doi: [10.1111/j.1365-2478.2007.00597.x](https://doi.org/10.1111/j.1365-2478.2007.00597.x).
- Porsani, M. J., and B. Ursin, 1998, Mixed-phase deconvolution: *Geophysics*, **63**, 637–647, doi: [10.1190/1.1444363](https://doi.org/10.1190/1.1444363).
- Porsani, M. J., and B. Ursin, 2000, Mixed-phase deconvolution and wavelet estimation: *The Leading Edge*, **19**, 76–79, doi: [10.1190/1.1438464](https://doi.org/10.1190/1.1438464).
- Robinson, E. A., 1957, Predictive decomposition of seismic traces: *Geophysics*, **22**, 767–778, doi: [10.1190/1.1438415](https://doi.org/10.1190/1.1438415).
- Robinson, E. A., 1967, Predictive decomposition of time series with application to seismic exploration: *Geophysics*, **32**, 418–484, doi: [10.1190/1.1439873](https://doi.org/10.1190/1.1439873).
- Robinson, E. A., and O. M. Osman, 1996, *Deconvolution 2: Society of Exploration Geophysicists*.
- Robinson, E. A., and S. Treitel, 1980, *Geophysical Signal Analysis*: Prentice-Hall.
- Sacchi, M. D., and T. J. Ulrych, 2000, Nonminimum-phase wavelet estimation using higher order statistics: *The Leading Edge*, **19**, 80–83, doi: [10.1190/1.1438466](https://doi.org/10.1190/1.1438466).
- Sen, M. K., and P. L. Stoffa, 1995, *Global Optimization Methods in Geophysical Inversion*: Elsevier.
- Taner, M. T., F. Koehler, and R. E. Sheriff, 1979, Complex seismic trace analysis: *Geophysics*, **44**, 1041–1063, doi: [10.1190/1.1440994](https://doi.org/10.1190/1.1440994).
- Treitel, S., and E. A. Robinson, 1966, The Design of High-Resolution Digital Filters: *IEEE Transactions on Geoscience Electronics*, **4**, 25–38, doi: [10.1109/TGE.1966.271203](https://doi.org/10.1109/TGE.1966.271203).
- Ulrych, T., and S. Treitel, 1991, A new proof of the minimum phase property of the unit delay prediction error operator-revisited: *IEEE Transactions on Signal Processing*, **39**, 252–254, doi: [10.1109/78.80799](https://doi.org/10.1109/78.80799).
- Ulrych, T. J., D. R. Velis, and M. D. Sacchi, 1995, Wavelet estimation revisited: *The Leading Edge*, **14**, 1139–1143, doi: [10.1190/1.1437089](https://doi.org/10.1190/1.1437089).
- Ulrych, T. J., and C. Walker, 1982, Analytic minimum entropy deconvolution: *Geophysics*, **47**, 1295–1302, doi: [10.1190/1.1441389](https://doi.org/10.1190/1.1441389).
- Ursin, B., J. Neto, and M. Porsani, 1996, Seismic reflection estimation with coloured noise: *Journal of Seismic Exploration*, **5**, 51–62.
- Ursin, B., and M. J. Porsani, 2000, Estimation of an optimal mixed-phase inverse filter: *Geophysical Prospecting*, **48**, 663–676, doi: [10.1046/j.1365-2478.2000.00206.x](https://doi.org/10.1046/j.1365-2478.2000.00206.x).
- van der Baan, M., 2008, Time-varying wavelet estimation and deconvolution by kurtosis maximization: *Geophysics*, **73**, V11–V18, doi: [10.1190/1.2831936](https://doi.org/10.1190/1.2831936).
- Wiggins, R. A., 1978, Minimum entropy deconvolution: *Geophysical Prospecting*, **16**, 21–35, doi: [10.1016/0016-7142\(78\)90005-4](https://doi.org/10.1016/0016-7142(78)90005-4).
- Yilmaz, Ö., 2001, *Seismic Data Analysis. Investigations in Geophysics*: Society of Exploration Geophysicists. (doi: [10.1190/1.9781560801580](https://doi.org/10.1190/1.9781560801580)).
- Ziolkowski, A., and E. Slob, 1991, Can we perform statistical deconvolution by polynomial factorization?: *Geophysics*, **56**, 1423–1431, doi: [10.1190/1.1443162](https://doi.org/10.1190/1.1443162).

Porsani M.J.: was responsible for the development of the phase-shrinkage filtering method, the implementation, and the testing of the algorithms, as well as for the writing and generation of the figures and results presented in the article.

Received on July 31, 2022 / Accepted on September 30, 2022



- Creative Commons attribution CC BY